Journal of Chromatography A, 1218 (2011) 6489–6497

Contents lists available at ScienceDirect

Journal of Chromatography A

journal homepage: www.elsevier.com/locate/chroma

Structure–transport correlation for the diffusive tortuosity of bulk, monodisperse, random sphere packings

Siarhei Khirevich[a], Alexandra Höltzel[a], Anton Daneyko[a], Andreas Seidel-Morgenstern[b], Ulrich Tallarek[a,*]

[a] Department of Chemistry, Philipps-Universität Marburg, Hans-Meerwein-Strasse, 35032 Marburg, Germany
[b] Max-Planck-Institut für Dynamik komplexer technischer Systeme, Sandtorstrasse 1, 39106 Magdeburg, Germany

ARTICLE INFO

Article history:
Received 1 April 2011
Received in revised form 11 July 2011
Accepted 12 July 2011
Available online 24 July 2011

Keywords:
Effective diffusion and tortuosity
Porosity scaling
Packing method and disorder
Degree of heterogeneity
Voronoi volume distribution
Delaunay tessellation

ABSTRACT

The mass transport properties of bulk random sphere packings depend primarily on the bed (external) porosity ε, but also on the packing microstructure. We investigate the influence of the packing microstructure on the diffusive tortuosity $\tau = D_m/D_{eff}$, which relates the bulk diffusion coefficient (D_m) to the effective (asymptotic) diffusion coefficient in a porous medium (D_{eff}), by numerical simulations of diffusion in a set of computer-generated, monodisperse, hard-sphere packings. Variation of packing generation algorithm and protocol yielded four Jodrey–Tory and two Monte Carlo packing types with systematically varied degrees of microstructural heterogeneity in the range between the random-close and the random-loose packing limit ($\varepsilon = 0.366$–0.46). The distinctive tortuosity–porosity scaling of the packing types is influenced by the extent to which the structural environment of individual pores varies in a packing, and to quantify this influence we propose a measure based on Delaunay tessellation. We demonstrate that the ratio of the minimum to the maximum void face area of a Delaunay tetrahedron around a pore between four adjacent spheres, $(A_{min}/A_{max})_D$, is a measure for the structural heterogeneity in the direct environment of this pore, and that the standard deviation σ of the $(A_{min}/A_{max})_D$-distribution considering all pores in a packing mimics the tortuosity–porosity scaling of the generated packing types. Thus, $\sigma(A_{min}/A_{max})_D$ provides a structure–transport correlation for diffusion in bulk, monodisperse, random sphere packings.

1. Introduction

The transport properties of porous media are a central theme of research in physics, chemistry, geology, and engineering, affecting such diverse fields as, *e.g.*, molecular diffusion in supercooled liquids and glasses, chemical separations by chromatography, migration of soil pollutants, and dam building. The ability to relate the transport properties of a porous medium to its pore space architecture is of fundamental interest [1,2]. Traditionally, structure–transport correlations for porous media were established from fitting experimental data or by using specific, simplified (often 2D) models to solve the fundamental transport equations. Structural properties of the porous medium were described by macroscopic, experimentally accessible parameters, such as density or porosity of the porous medium. In chromatography, we have come to rely on the bed or external porosity ε (interparticle void volume fraction) of particle-packed columns as one of the most important parameters to estimate column quality, because two important mass transport properties, hydraulic permeability and hydrodynamic dispersion, depend first and foremost on the bed porosity [3]. However, the common wisdom of chromatographers that dense, well-packed beds make good columns, also includes the homogeneity of the packing microstructure as a significant factor for the column performance. Between two columns of equal bed porosity, the column with the more homogeneous packing has a lower hydrodynamic dispersion coefficient and will thus yield better separation efficiency. The impact of microstructural heterogeneity may even overpower the influence of the bed porosity. This effect has been observed in recent chromatographic practice for columns packed with core–shell particles [4]. These columns pair exceptionally low plate heights with rather high bed porosities (typically $\varepsilon = 0.40$–0.43), a combination not observed for the traditional, fully porous particles. The low plate heights are mainly due to a low eddy dispersion contribution to band broadening, which is attributed to a homogeneous packing microstructure [5–7].

Systematic knowledge about structure–transport correlations for particulate packings has been derived from numerical simulations of flow and transport in computer-generated random sphere packings [8–10] as well as the just recently demonstrated

* Corresponding author. Tel.: +49 6421 28 25727; fax: +49 6421 28 27065.
E-mail address: tallarek@staff.uni-marburg.de (U. Tallarek).
URL: http://www.uni-marburg.de/fb15/ag-tallarek (U. Tallarek).

0021-9673/$ – see front matter © 2011 Elsevier B.V. All rights reserved.
doi:10.1016/j.chroma.2011.07.066

physical reconstruction of the morphology of modern chromatographic supports [11,12]. From numerical simulation studies of bulk, monodisperse, random sphere packings [10] we know that (i) the hydrodynamic axial dispersion coefficient D_{ax} increases with the bed porosity and with the degree of heterogeneity (DOH) of the packing microstructure; (ii) the larger the DOH of a packing microstructure, the steeper the increase of D_{ax} with increasing bed porosity; (iii) the DOH of a packing microstructure may be captured by Voronoi tessellation and is related to the second and third statistical moments (standard deviation and skewness) of the Voronoi volume distribution; and (iv) the hydrodynamic dispersion coefficient depends mainly on the short-range interchannel contribution to eddy dispersion originating in the packing's short-range disorder on the length scale of 1–2 particle diameters, specifically the parameters λ_2 and ω_2 as defined by Giddings [9,10,13], which scale with the standard deviation and skewness of the Voronoi volume distributions. Another possibility to describe the DOH of a packing microstructure is the determination and analysis of chord length distributions of the packing void space [12]. The chord length distribution of experimental, physically reconstructed packings follows a two-parameter distribution function (a simplified *k*-gamma function): the parameter of location (arithmetic mean) provides an alternative measure for pore size, which is crucial to column efficiency; the average pore size of a column correlates with transchannel dispersion. The *k*-value obtained from the chord length distributions is a second-moment parameter that defines the (statistical) dispersion of the distribution function, and therefore is a descriptor of packing-scale disorder. It provides a scalar measure for pore heterogeneity on the length scale of short-range interchannel (hydrodynamic) dispersion. Thus, we have two different methods to describe the microstructural DOH of a packing, one based on Voronoi tessellation, the other based on chord length distributions [10,12].

Because eddy dispersion and ultimately band-broadening are of central importance in chromatography, much less thought is usually given to other transport properties such as hydraulic permeability and effective diffusion in a packing. The diffusion coefficient appears in the plate height equation in form of the obstruction factor γ, defined as [13]

$$\gamma = \frac{D_{\mathrm{eff}}}{D_{\mathrm{m}}} = \lim_{t\to\infty} \frac{D(t)}{D_{\mathrm{m}}} = \frac{1}{\tau}, \quad (1)$$

where D_{m} is the molecular diffusion coefficient in bulk solution, $D(t)$ is the pre-asymptotic molecular diffusion coefficient in the porous medium, and D_{eff} is its effective, *i.e.*, asymptotic (long-time) value; the inverse of the obstruction factor is the *diffusive tortuosity* τ. The obstruction factor γ, which directly states the extent to which free diffusion of a molecule in solution is hindered (obstructed) by the presence of the solid obstacles in a porous medium, has the merit of being an illustrative descriptor, but its use is mainly confined to chromatography. The wider scientific community prefers the term tortuosity, which recalls the winding of the fluid pathways through a porous medium. Unfortunately, several conflicting definitions of tortuosity are in use, as pointed out in [14,15]. For example, the often used definition of tortuosity as the ratio between the average length of a crooked path between two points to the straight distance, is a purely geometric parameter whose value is easily determined for a model of unconnected, twisted tubes of constant cross-section, but not for a real, complex porous medium. In contrast, definitions of tortuosity that are based on experimentally accessible quantities, such as electric and diffusive tortuosity, are physically meaningful as well as unequivocal, as they do not depend on a specific structural model of the porous medium.

Tortuosity is a very important topic in the general research on porous media, and the idea to predict the tortuosity of a porous medium from its porosity – beginning with Maxwell's equation dating back to the last quarter of the 19th century [16] – has produced a steady stream of propositions for tortuosity–porosity correlations, based on empirical data or theoretical models [17,18]. The existing correlations differ in their definition of tortuosity, but generally describe it as a decreasing function of porosity. Although the diversity of porous media precludes the existence of a universal tortuosity–porosity correlation, the notion exists that such an equation could be found for a well-defined porous medium such as a random packing of hard objects of equal shape [19]. Several correlations for such packings have been proposed [16,19–28], all of them basically more or less elaborate functions of the bed porosity. Although these correlations implicitly account for the packing microstructure through the underlying model used for the porous medium, they nonetheless convey the message that the tortuosity of a random packing of uniform, hard spheres is fully determined by the bed porosity. In fact, the question if random sphere packings of equal bed porosity, but different packing microstructure, could differ in their tortuosities and moreover, in their tortuosity–porosity scaling, as known for crystal packings [29,30], has to our knowledge never been posed nor investigated. Thus, the published literature on porous media gives the impression that as far as tortuosity is concerned there are different types of crystal (*i.e.*, ordered) sphere packings, but only one type of random sphere packing.

In this work, we investigate the tortuosity–porosity scaling of bulk, monodisperse, random hard-sphere packings that differ only in the individual arrangement of the obstacles to find a structure–transport correlation for diffusion. By variation of packing generation algorithm and parameters, we computer-generated six distinct packing types over a bed porosity range of $\varepsilon = 0.366$–0.46, *i.e.*, from random-close to random-loose packing. We simulate diffusion in the void space of the packings by a random-walk particle-tracking technique, and then compute the diffusive tortuosity values for each packing type and porosity to evaluate how the resulting tortuosity–porosity curves reflect the different packing types.

2. Numerical simulations

2.1. Packing generation

Isotropic, random, unconfined packings of monosized, uniform, hard, impermeable spheres were computer-generated with dimensions of approximately $10 \times 10 \times 70$ sphere diameters (d_{p}), applying periodic boundary conditions in all directions. The packing dimensions were chosen originally for the analysis of hydrodynamic dispersion [10], where long packings are required to observe asymptotic behavior. Although shorter packings would suffice to observe asymptotic diffusion behavior, we used the long packings to extend the sample size, *i.e.*, the long packings count as several realizations of shorter packings.

Four packing types were generated using a modified Jodrey–Tory (JT) algorithm [31], a collective-rearrangement method [32], which yields geometrically jammed, but mechanically unstable packings. The relevant properties of the JT-algorithm for this study are: (i) it yields isotropic packings, (ii) partial crystallization is avoided [33], (iii) bed porosity and DOH can be systematically varied through the generation parameters [10]. Please note that isotropy at the packing scale does not exclude the presence of local anisotropy [34]. Packing generation with the JT-algorithm starts from a random distribution of sphere centers in a simulation box, where sphere overlap is typical. Each iteration includes the search for two sphere centers with a minimum pair-wise distance that defines the maximal sphere diameter at which no sphere-overlap occurs in the current configuration, followed by symmetrical displacement of the two sphere cen-

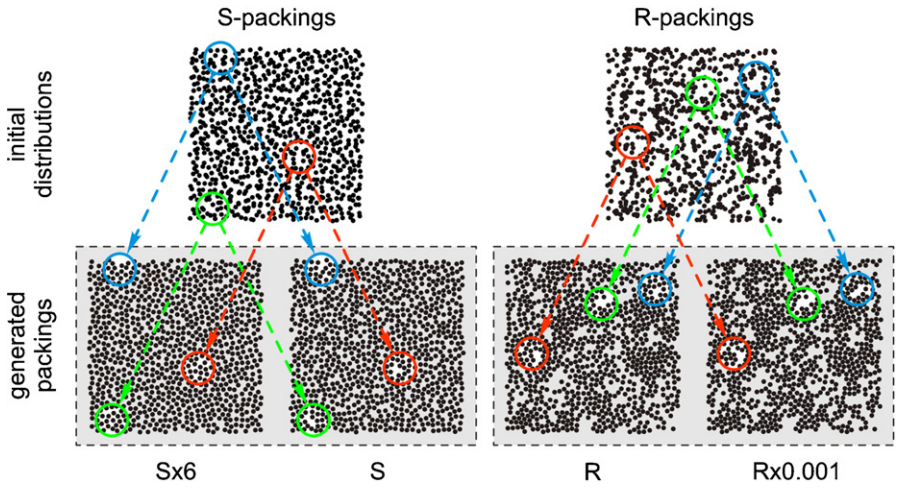

Fig. 1. Bulk (unconfined) random packings of monosized hard disks at $\varepsilon \approx 0.46$ generated with the Jodrey–Tory algorithm following different packing protocols. Shown are the initial distributions of the disks for S- and R-configurations (top) and the generated two-dimensional packings (Sx6, S, R, Rx0.001; bottom). Colored circles aid the comparison between initial and final packing microstructure. (For interpretation of the references to color in this figure legend, the reader is referred to the web version of the article.) The figure is reproduced from [10].

ters up to a new distance. The displacement length used in the second step is scaled by a constant α. Different JT-packing types were generated by (i) varying the initial distribution scheme of the sphere centers and (ii) the value of the constant α scaling the displacement length [10]. Generation of R-packings started from a random and uniform distribution of sphere centers in the simulation box, whereas for S-packings the simulation box was first divided into equal cubes and then each sphere center placed in a random position into a cube. The scaling constant was set to $\alpha = 0.001$ (Rx0.001), $\alpha = 1$ (R and S), or $\alpha = 2$ (Sx2). With a small displacement length sphere centers remain close to their initial positions during packing generation, preserving the randomness of the initial distribution. A larger displacement length yields a more homogeneous distribution of sphere centers in the final configuration (Fig. 1).

The Monte Carlo (MC) algorithm provides a complementary approach to the JT algorithm for generating dense, random sphere packings [35]. MC-packing generation starts from a uniform distribution of spheres in a dilute cubic array constructed from expanding a simple cubic lattice. We used an expansion factor of 2, resulting in an eight times larger volume of the initial packing compared with a simple cubic packing. The packing spheres are moved in random directions, and each move that does not result in a collision with another sphere is accepted. The desired bed porosity ε is reached by compression of the coordinate system, executed every 5000 movement attempts and scaled by a compression rate Ω [36]. By using $\Omega = 0.95$ (fast compression) or $\Omega = 0.05$ (slow compression), we generated two different MC-packing types, Ωx0.95 and Ωx0.05, respectively. The values were chosen from the ends of the possible range ($0 < \Omega \leq 1$) to create a maximum of microstructural variety with the two MC-packing types.

Each packing type was generated at six porosities ($\varepsilon = 0.366$, 0.38, 0.40, 0.42, 0.44, 0.46) with one exception: we were not able to generate Sx2-packings at $\varepsilon = 0.366$. To account for statistical variations, ten realizations (in consideration of the available computational resources) of each packing type and porosity were generated, 350 packings in total. Results reported for a packing of a given type and porosity refer to the mean value from the ten individual realizations. The number of realizations together with the extended packing dimensions ensured a thorough sampling of the structural variations among individual packings of the same type and porosity.

2.2. Simulation of diffusion

Diffusion in the generated packings was simulated by a random-walk particle-tracking technique [37], employing a multiple rejection boundary condition at the solid–liquid interface [38]. An ensemble of 5×10^6 inert, point-like tracer particles was randomly distributed within the void space of a packing, and then displaced due to random motion calculated from a Gaussian distribution with a mean of zero and a variance of $(2D_m\delta t)^{1/2}$ (where D_m is the diffusion coefficient of the tracer particles in bulk solution) around each spatial coordinate. The position of all tracers was monitored at each time step δt, defined such that the maximum tracer displacement at each iteration did not exceed a distance of $d_p/60$. Diffusion coefficients $D(t)$ in a given direction were calculated from the tracer displacements [39] as

$$D_x(t) = \frac{1}{2N}\frac{d}{dt}\sum_{i=1}^{N}(\Delta r_{xi} - \langle \Delta r_x \rangle)^2, \quad (2)$$

where Δr_{xi} and $\langle \Delta r_x \rangle$ denote the corresponding Cartesian components of the displacement of the ith tracer and the average displacement of the tracer ensemble after time t, respectively, in x-direction. Isotropic diffusion behavior was observed for all packing types. The effective diffusion coefficients D_{eff} were determined from the asymptotes of the $D(t)/D_m$-curves (shown for selected packings in Fig. 2), and tortuosity values τ calculated from Eq. (1).

To represent the boundaries of the packings' spheres, we used a smoothed spheres approach [40], where discretization is omitted and random walk takes place between spheres with smooth as opposed to stair-step contours. The adequate geometrical representation of the spherical obstacles in the packing is important for modeling diffusion, because the path of a tracer around a ragged surface is longer than around a smooth one, which results in exaggerated tortuosity values.

For comparison, effective diffusion was also simulated in three crystal packing types, the face-centered cubic (FCC), the body-centered cubic (BCC), and the hexagonal close-packed (HCP) structure. To obtain crystal packings with bed porosities within the investigated range of $\varepsilon = 0.366$–0.46, the crystal structures were uniformly diluted.

The program realization of all algorithms was implemented as parallel codes in C language using the Message Passing Interface (MPI) library [41]. Total simulation time for all packings was ~110 h

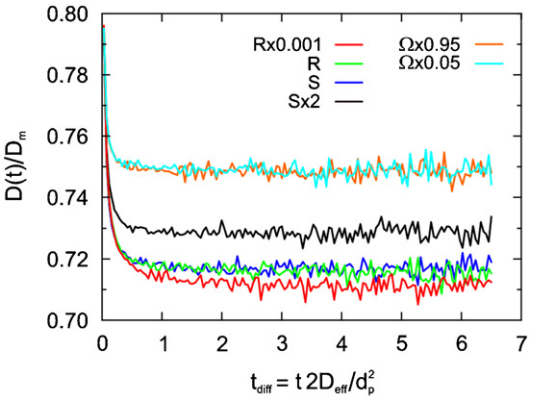

Fig. 2. Time-evolution of the normalized diffusion coefficient $D(t)/D_m$ for selected packings at $\varepsilon = 0.46$ for simulations of diffusion with the smoothed spheres approach. Elapsed time is given in units of the diffusive time, defined as $t_{diff} = t2D_{eff}/d_p^2$, where D_{eff} is the long-time (asymptotic) value of the diffusion coefficient in a sphere packing and d_p is the sphere diameter. One diffusive time unit is the time it takes for a tracer to travel a distance equal to one sphere diameter by diffusion.

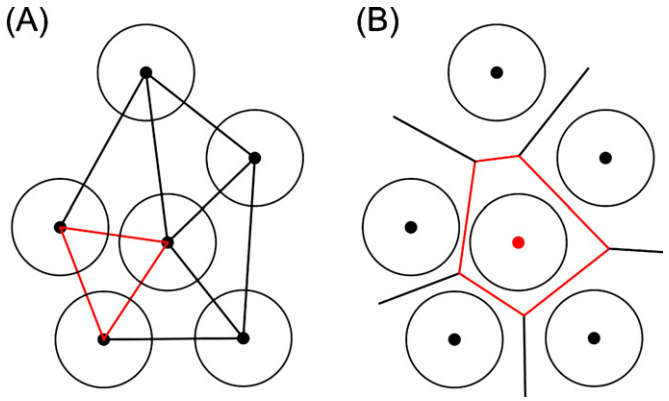

Fig. 4. Spatial tessellation of a two-dimensional packing of uniform disks. (A) Delaunay tessellation. (B) Voronoi tessellation.

on 2048 BlueGene/P processor cores. For Voronoi and Delaunay tessellations [42] of the generated packings we used MATLAB7.0 built-in routines, which are based on the Quickhull algorithm introduced by Barber et al. [43].

3. Results and discussion

3.1. Packing generation and microstructure

By variation of the packing generation algorithm and parameters, we generated a set of six distinct types of monodisperse, bulk, random sphere packings at bed (external or interparticle) porosities of $\varepsilon = 0.366$–0.46. These packings mimic infinitely wide, randomly packed beds of hard, impermeable, uniform spheres without confining walls. To illustrate the effect of the varied packing generation parameters on the final packing microstructure, we use a two-dimensional representation, *i.e.*, random packings of uniform disks instead of spheres. Fig. 1 visualizes the two-step parameter variation used for packing generation with the Jodrey–Tory (JT)-algorithm to yield the four JT-packing types Rx0.001, R, S, and Sx2. (The Sx2-packing is replaced by a Sx6-packing in Fig. 1 to achieve a stronger visual effect.) S-packing generation starts from a more ordered (lattice-based) initial distribution of sphere centers than R-packing generation, and the value of the constant for scaling the displacement length $\alpha = 6$ (2 for sphere packings), 1, or 0.001 determines how well inhomogeneities in the initial distribution of sphere centers are balanced out in the final packing microstructure. It is important to recognize from Fig. 1 that the parameter variation used with the JT-algorithm operates on two different length scales: the initial ordered or random distribution of the sphere centers concerns the whole packing, whereas the value of the scaling constant α affects the local environment of the individual spheres in the packing.

The varied parameter in packing generation with the Monte Carlo (MC)-scheme was the value of the compression rate Ω; using a high ($\Omega = 0.95$) and a low ($\Omega = 0.05$) value for the compression rate yielded the two MC-packing types Ωx0.95 and Ωx0.05, respectively. The MC-algorithm is known to incorporate highly ordered, densely packed regions into a packing, if low compression rates and low bed porosities are combined [8,33]. Fig. 3 illustrates the effect of the compression rate value on the final packing microstructure for disk packings generated with high ($\Omega = 0.99$) and low ($\Omega = 0.025$) compression rates. The amount of densely packed regions in a packing can be estimated by Delaunay tessellation. Delaunay tessellation divides the three-dimensional packing space into a mesh by taking the centers of four next-neighbor spheres as the vertices of a tetrahedron [42]. In the two-dimensional case, connecting the centers of next-neighbored disks yields a Delaunay mesh of triangles (Fig. 4A). In highly ordered regions, disks form close-to-regular triangles on the Delaunay mesh. A suitable estimate for the deviation from regularity of a Delaunay triangle is its maximum edge length Δ_{max} [44]. Delaunay triangles with maximum edge length smaller than a certain critical value of Δ_{max} are considered to indicate a highly ordered, densely packed region. In Fig. 3 we show the results for applying a stricter ($\Delta_{max} < 1.06d_d$, where d_d is the disk diameter) as well as a looser ($\Delta_{max} < 1.09d_d$) criterion. While a looser criterion naturally increases the amount of densely packed regions in both packings, the MC-packing generated with a low compression rate ($\Omega = 0.025$) contains a higher fraction of such

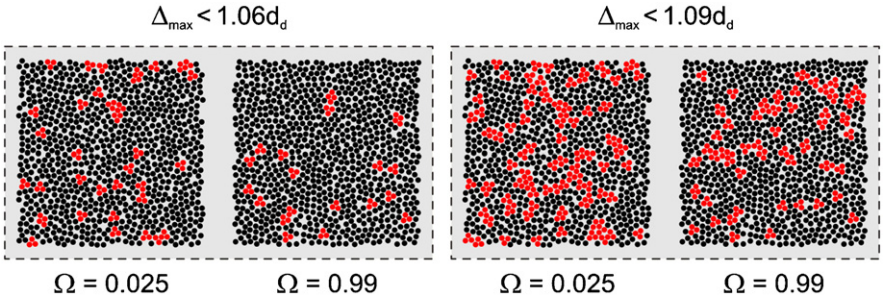

Fig. 3. Effect of the compression rate value Ω on the microstructure of bulk random packings of monosized disks at $\varepsilon \approx 0.34$ generated with a Monte Carlo-scheme. Closely packed regions are colored red. Closely packed disks form close-to-regular triangles on a Delaunay mesh (resulting from connecting the centers of adjacent disks), and were identified by the value of the maximum edge length Δ_{max} of the triangles, with $\Delta_{max} < 1.06d_d$ (where d_d is the disk diameter; left) or $\Delta_{max} < 1.09d_d$ (right). (For interpretation of the references to color in this figure legend, the reader is referred to the web version of the article.)

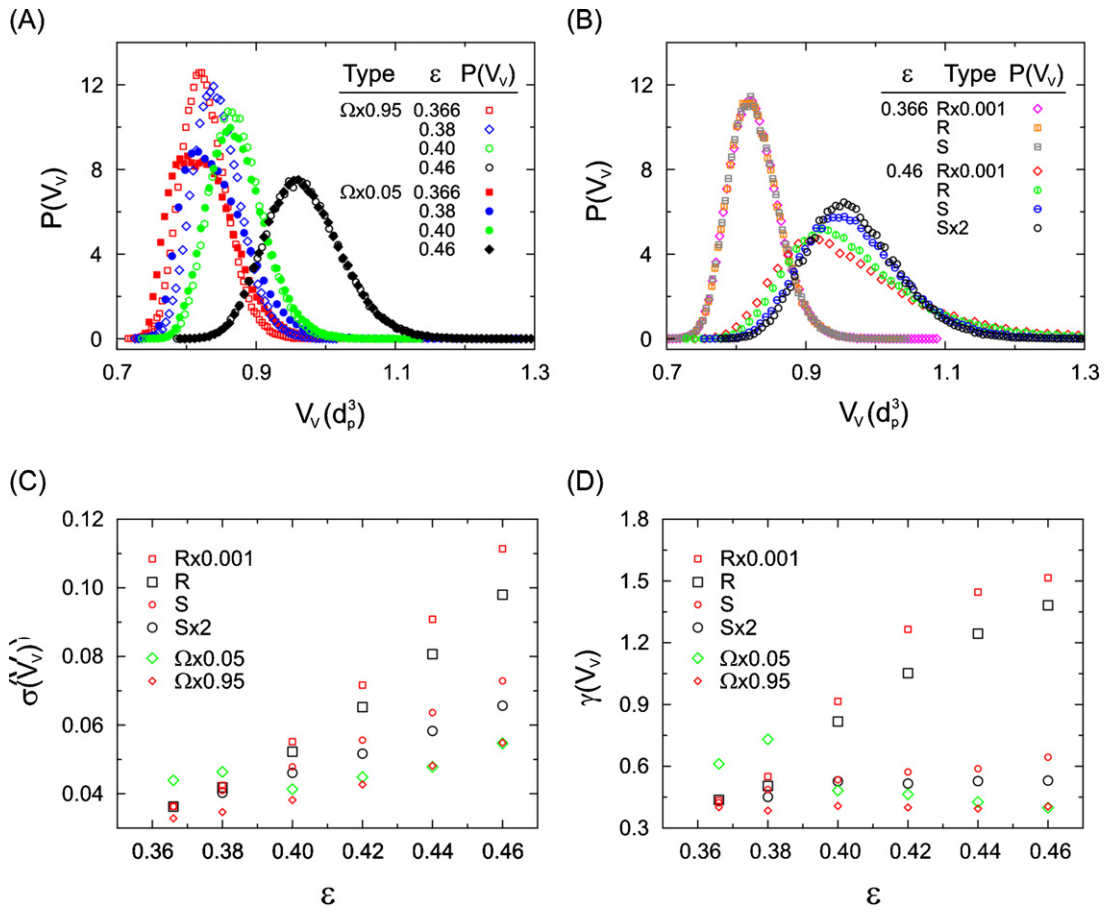

Fig. 5. Voronoi volume distributions of the generated Monte Carlo (A) and Jodrey–Tory (B) packings at selected bed porosities. Standard deviation (C) and skewness (D) of the Voronoi volume distributions of the generated packings as a function of bed porosity. Panel (B) is reproduced from [10].

regions than the MC-packing generated with the high compression rate ($\Omega = 0.99$) for both values of Δ_{max}.

Each of the generated packings has a microstructure that depends on packing type and bed porosity and whose degree of heterogeneity (DOH) can be determined by Voronoi tessellation [10]. Voronoi tessellation surrounds each sphere in a monodisperse packing by a polyhedron that contains all points closer to this sphere center than to any other (Fig. 4B). The packing space is thus divided into a set of non-overlapping polyhedra with associated Voronoi volumes V_V [42]. The V_V-distributions for the generated packing types at selected porosities are shown in Fig. 5A and B. For JT-packings, the V_V-distributions are generally unimodal (Fig. 5B). The identical V_V-distributions of the JT-packing types at $\varepsilon = 0.366$ reflect the severely restricted possibilities for the placement of individual spheres at the random-close packing limit: at this limiting density, Rx0.001-, R-, and S-packings have identical microstructures (within the limits of statistical variation). With increasing bed porosity the V_V-distributions widen and shift to larger values, and differences between the packing types emerge, until at the random-loose packing limit ($\varepsilon = 0.46$), the V_V-distributions reflect most clearly the respective JT-packing types (Fig. 1): the most homogeneous packing type has the narrowest and most symmetrical distribution (Sx2), and the most heterogeneous packing type the widest and most skewed distribution (Rx0.001).

MC-packings show the opposite trend to the JT-packings in the porosity-scaling of their V_V-distributions (Fig. 5A): both MC-packing types have identical, unimodal, symmetrical distributions at $\varepsilon = 0.46$, and differ most from each other at $\varepsilon = 0.366$, where the Ωx0.95-packing has a narrow, symmetrical V_V-distribution, whereas that of the Ωx0.05-packing is widened and skewed due to a developing second mode at smaller volumes. The latter V_V-distribution reflects a microstructure composed of dense, highly ordered regions (associated with smaller Voronoi volumes) interspersed between more loosely packed regions (associated with larger Voronoi volumes), the result of combining low bed porosity and low compression rate during packing generation with the Monte Carlo-scheme (*cf.* Fig. 3).

Fig. 5C and D, which shows standard deviation and skewness, respectively, of the V_V-distributions for the generated packings, quantify and summarize the information gained from Fig. 5A and B. The two parameters $\sigma(V_V)$ and $\gamma(V_V)$ are a quantitative measure for the microstructural DOH of a packing and follow the same porosity-scaling as the hydrodynamic dispersion coefficient [10]. Each of the six packing types has a unique porosity-scaling of the DOH. For the four JT-packing types it reflects their relative packing-scale disorder: Rx0.001 > R > S > Sx2, *i.e.*, the higher the packing-scale disorder, the higher the value of $\sigma(V_V)$ and $\gamma(V_V)$ at a given porosity and the steeper the rise of these two parameters at increasing porosity. MC-packings are more homogeneous than the most homogeneous JT-packing type (Sx2) at high to intermediate porosities ($\varepsilon = 0.46$–0.40), and for the Ωx0.95-packing type this remains the case also at low bed porosities ($\varepsilon = 0.38$–0.366). Considering that MC-packing generation starts from a lattice-based distribution of sphere centers, this result is not unexpected. Whereas the Ωx0.95-packing type follows essentially the same trend upon densification as the JT-packing types, *i.e.*, the DOH decreases, only with a smaller slope, the Ωx0.05-packing type behaves quite differently: its DOH goes through a minimum at $\varepsilon = 0.40$ and then increases again, so that at $\varepsilon = 0.366$ the Ωx0.05-packing has the highest DOH among all packing types. This high DOH is explained by the irregular distri-

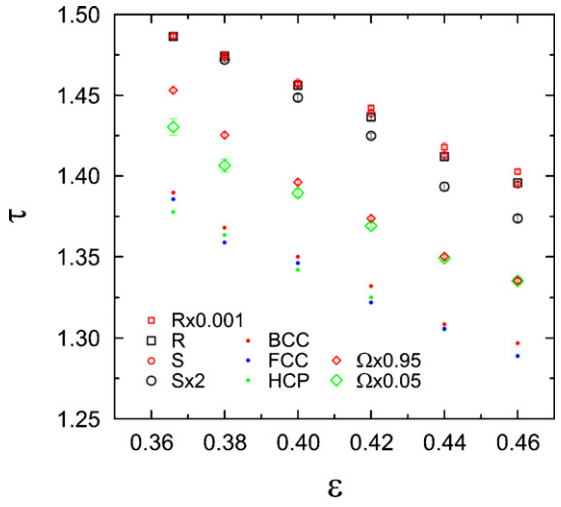

Fig. 6. Tortuosity–porosity scaling of the generated packing types. Statistical variations among ten individual random sphere packings of a given type and porosity are expressed by 95% confidence intervals calculated using the standard error of the mean. Also shown are tortuosity values simulated for three crystal packing types: the body-centered cubic (BCC), face-centered cubic (FCC), and hexagonal close-packed (HCP) structure.

bution of dense and more loosely packed regions, which translates to increased disorder on the packing scale.

3.2. Tortuosity–porosity scaling of the generated packing types

The tortuosity–porosity data in Fig. 6 present the results of simulating effective diffusion in the void space of the generated packings. At first glance, the tortuosity–porosity data of the JT-packing types reflect their relative packing-scale disorder (Fig. 5C and D), with identical tortuosity values ($\tau = 1.486$) at $\varepsilon = 0.366$ and maximum difference at $\varepsilon = 0.46$, where the most homogeneous JT-packing type (Sx2) has the lowest tortuosity ($\tau = 1.373$) and the most heterogeneous JT-packing type (Rx0.001) the highest tortuosity ($\tau = 1.403$). R- and S-packings, however, have *identical* tortuosities (within statistical variation) throughout the investigated porosity range. Because the common parameter in their generation is the value for the displacement length scaling-constant ($\alpha = 1$), the identical tortuosity–porosity curves of R- and S-packings suggest that the influence of the packing microstructure on diffusion is restricted to the operative length scale of α, *i.e.*, to the *local* environment of individual spheres. Expressed in terms of the packing void space, the value of α affects the pores and the pathways to adjacent pores, the pore throats.

MC-packings are generally less tortuous than JT-packings, with tortuosity values between $\tau = 1.335$ at $\varepsilon = 0.46$ and $\tau = 1.430$ (Ωx0.05) or $\tau = 1.454$ (Ωx0.95) at $\varepsilon = 0.366$. Differences between the two MC-packing types emerge and increase upon densification as was observed for the DOH (Fig. 5C and D), but the Ωx0.05-packing type maintains the *lowest* tortuosity among all generated packing types throughout the whole porosity range. This contrasts with the observation that at low porosities ($\varepsilon = 0.38$ and 0.366) the Ωx0.05-packing type has the largest DOH of all generated packing types (Fig. 5C and D), and is thus another indicator that the packing-scale disorder is not the determining factor for tortuosity.

Fig. 6 demonstrates that the microstructure of bulk, monodisperse, random sphere packings influences the diffusive tortuosity. Although the effect is small – 2% difference between the extreme JT-packing types Sx2 and Rx0.001 at $\varepsilon = 0.46$, and similarly *ca.* 2% difference between the two MC-packing types at $\varepsilon = 0.366$ – it is genuine and not due to statistical variations among individual packings of a given type and porosity, as the small confidence intervals in Fig. 6 prove.

Table 1
Values received for p and correlation coefficients R^2 from fitting the tortuosity–porosity data simulated for the generated packing types to the modified Weissberg equation (Eq. (4)).

Packing type	p	R^2
Rx0.001	0.499	0.876
R	0.496	0.943
S	0.496	0.938
Sx2	0.486	0.989
Ωx0.95	0.436	0.966
Ωx0.05	0.425	0.990

Also interesting is the contrast to the crystal packings, whose simulated tortuosities already approach the analytical solutions [29]. The tortuosity values of MC-packings lie between those of JT- and the crystal packing types, which again reflects the lattice-based distribution of sphere centers from which MC-packing generation starts. Fig. 6 graphically depicts that in the investigated porosity range there may be more variety in tortuosity values between different types of random sphere packings than between different types of crystal packings!

According to Fig. 6 a tortuosity–porosity relation for random sphere packings needs to consider the influence of the packing microstructure. One of the earliest correlations was proposed on a theoretical basis by Weissberg [20] as a lower bound for the tortuosity in random arrangements of freely overlapping spheres:

$$\tau = 1 - 0.5 \cdot \ln \varepsilon. \quad (3)$$

In its modified form,

$$\tau = 1 - p \cdot \ln \varepsilon, \quad (4)$$

Weissberg's correlation has found corroboration from experiments [14,17,21] as well as simulations [19], with values of $p = 0.49$ [14,21], $p = 0.77$ [19], and $p = 2$ [17]. Theoretical correlations are derived for a specific model structure and are thus in principle restricted in their applicability. The reason for the popularity of the modified Weissberg correlation lies probably in its elegant simplicity and easy adaptability through a variable coefficient, which allows to fit a wider range of packing types than more elaborate equations.

We fitted our simulated tortuosity–porosity data of Fig. 6 to Eq. (4), using p as an adjustable parameter. The results for p along with the correlation coefficients R^2 for the fits are listed in Table 1. For the Rx0.001, R-, and S-packing types we received $p \approx 0.5$, the value predicted by Weissberg [20], whereas the result for the Sx2-packing type is closer to $p = 0.49$, the value introduced by Mauret and Renaud [21]. MC-packings are set apart by smaller p-values ($p = 0.43$–0.44). If we rank the six packing types according to the relative position of their tortuosity curves in Fig. 6 as Ωx0.05 < Ωx0.95 < Sx2 < S,R < Rx0.001, the calculated p-values also increase in this sequence. Interestingly, the correlation coefficients show the opposite trend, *i.e.*, those packing types (Ωx0.05 and Sx2) whose generation parameters were intended to create homogeneous packing microstructures demonstrate the best adherence to the modified Weissberg equation. In summary, however, the correlation coefficients are unconvincing and lead to the conclusion that the tortuosity–porosity scaling of the generated packing types is not adequately represented by the modified Weissberg equation.

3.3. Geometrical representation of the packing pore space by Delaunay tessellation

The analysis of the tortuosity–porosity data for the different packing types in the previous section suggests that diffusion is

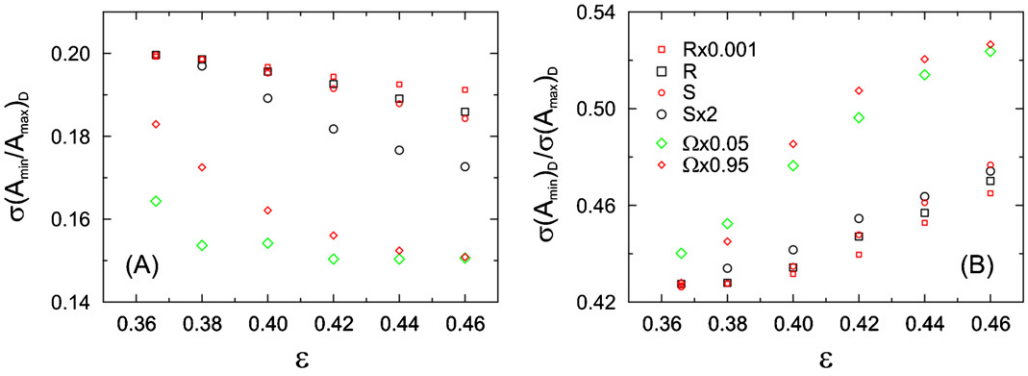

Fig. 7. Delaunay tessellation surrounds each pore in a packing with an irregular tetrahedron, whose faces have solid and void areas. (A) Porosity-scaling of $\sigma(A_{min}/A_{max})_D$, the standard deviation of the distribution that describes the ratio between the minimum and the maximum void face area of each Delaunay tetrahedron in the tessellated packing. (B) Porosity-scaling of $\sigma(A_{min})_D/\sigma(A_{max})_D$, the ratio of the standard deviations of the distributions for A_{min} and A_{max}.

influenced on a length scale approximately equal to the direct environment of individual pores in a packing. To find a suitable measure for the structural heterogeneity at this length scale, we employed Delaunay tessellation, because this method has been shown to be especially valuable for characterization of the packing void space [44–51]. Delaunay tessellation divides monodisperse sphere packings into irregular tetrahedra, whose vertices are the centers of four closest (but not necessarily touching) spheres that enclose a pore (*cf.* Fig. 4A). The packing space is completely filled with non-overlapping tetrahedra, each comprised of solid and void components: the void volume of a Delaunay tetrahedron represents the pore volume, and the void areas of the tetrahedron's four faces correspond to the cross-sections of the pore throats that form the connections to the four neighboring pores, *i.e.*, the entrance and exit ways for a tracer particle into or out of a given pore. We evaluated several metric properties of the Delaunay tetrahedra for their ability to represent the influence of the packing microstructure on the packings' tortuosity: volume; maximum, minimum, and average void face areas; maximum, minimum, and average edge length; and the *T*-measure [44], which quantifies the deviation of the Delaunay tetrahedra from regularity (Delaunay simplices of the densest crystal packings, FCC and HCP, are perfect tetrahedra and quartoctahedra); also the distances of the center of mass to the center of the faces, as well as various combinations of the said metric properties. The mean, standard variation, and skewness of each metric property was calculated and its porosity-scaling compared to those of the simulated diffusive tortuosities. The mean of the maximum and the mean of the minimum void face area – but not that of the average void face area – gave close results, pointing to the limiting rather than the average properties of a pore as a possible measure. We found a good representation for the tortuosity–porosity scaling of all packing types by considering *two* limiting properties for each pore, namely the ratio of the minimum and maximum void face areas of each Delaunay tetrahedron $(A_{min}/A_{max})_D$. The diffusive probability for a tracer particle to move into or out of a given pore is determined by the size of the pathways to the pore, *i.e.*, by the pore throats, whose cross-sections are represented by the void areas of the Delaunay tetrahedron's four faces. We interpret the value of $(A_{min}/A_{max})_D$ as a measure for the heterogeneity in the direct environment of a single pore. In the limit of $(A_{min}/A_{max})_D = 1$, the pore environment is fully homogeneous, because all void face areas are equal, which means that the four pore throats through which a tracer could leave the pore have equal cross-sectional areas. The lower the value of $(A_{min}/A_{max})_D$, the more heterogeneous is the pore environment. If $(A_{min}/A_{max})_D$ is calculated for each Delaunay tetrahedron in a tessellated packing, the resulting distribution describes the different kinds of pore environments that exist in this packing. The standard deviation of this distribution, $\sigma(A_{min}/A_{max})_D$, has a porosity-scaling (Fig. 7A) that closely mimics that of the tortuosity values for each packing type (Fig. 6); thus, we propose $\sigma(A_{min}/A_{max})_D$ as a suitable descriptor for the influence of the packing microstructure on the diffusive tortuosity of monodisperse, bulk, random sphere packings.

The success of the identified measure, $\sigma(A_{min}/A_{max})_D$, lies in considering two limiting properties for each pore in the packing, before the standard deviation of the distribution is calculated. If the standard deviations of the two distributions for one limiting property of each individual pore are related, the resulting value, $\sigma(A_{min})_D/\sigma(A_{max})_D$, fails to mimic the tortuosity–porosity scaling of the different packing types (Fig. 7B). The comparison of Fig. 7A and B with Fig. 6 demonstrates the importance of relating two limiting properties for each pore to describe the heterogeneity around individual pores in a packing and ultimately the tortuosity. It also explains why previous attempts to correlate tortuosity with statistical moments of the pore size distribution or similar measures gave inconclusive results [51,52].

The $(A_{min}/A_{max})_D$-distributions reveal details about the changes in the direct pore environment upon densification of the different packing types. Fig. 8A shows $(A_{min}/A_{max})_D$-distributions for the JT-packings at the limiting bed porosities. The distributions are positively skewed and cover a range of *ca.* $(A_{min}/A_{max})_D = 0.05–1$. At $\varepsilon = 0.46$, the $(A_{min}/A_{max})_D$-distribution of the Rx0.001-packing is only minimally different from the two virtually identical $(A_{min}/A_{max})_D$-distributions of the R- and S-packing, whereas the distribution of the Sx2-packing is visibly shifted to larger $(A_{min}/A_{max})_D$-values. At $\varepsilon = 0.366$, the $(A_{min}/A_{max})_D$-distributions of the Rx0.001, R-, and S-packings are identical, just as previously observed for the Voronoi volume distributions (Fig. 5B), because at the random-close packing limit, the JT-packing types converge to the same microstructure. The two spikes that appear at $(A_{min}/A_{max})_D = 0.38$ and 1 coincide with the $(A_{min}/A_{max})_D$-values calculated for the FCC packing at its limiting porosity of $\varepsilon = 0.26$. The FCC packing has two Delaunay simplices of regular geometry, a tetrahedron and a quartoctahedron, which yield values of $(A_{min}/A_{max})_D = 1$ and 0.38, respectively. The latter line is not invariant with the porosity, but shifts to larger values upon dilution of the packing. A value of $(A_{min}/A_{max})_D = 1$ is also calculated for the BCC packing, where the underlying Delaunay simplex is a tetrahedron with equal faces (but not with equal edges, as in the FCC packing). Densification of JT-packing types (from $\varepsilon = 0.46$ to $\varepsilon = 0.366$) shifts the maximum of the $(A_{min}/A_{max})_D$-distribution to *larger* values and thus *more homogeneous* pore environments and raises

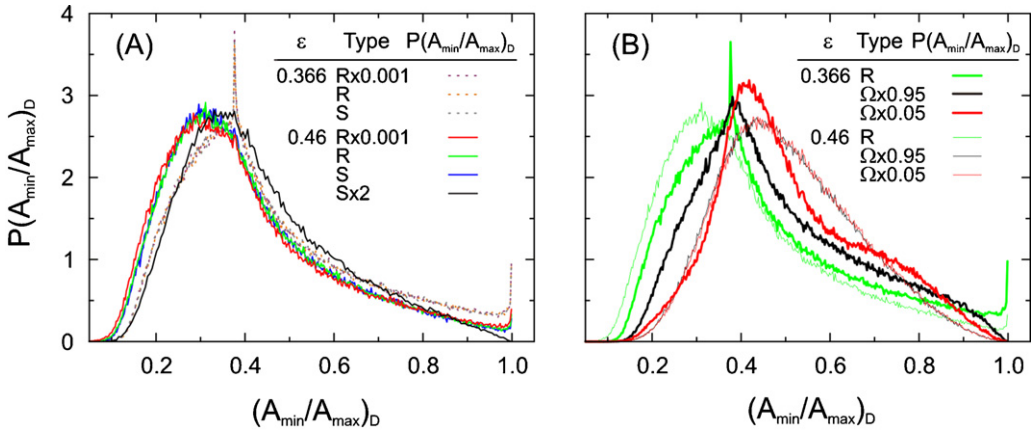

Fig. 8. Distribution of $(A_{min}/A_{max})_D$ for the generated packings at the limiting porosities. (A) Comparison of the Jodrey–Tory packing types. (B) Comparison of the Monte Carlo-packing types with the Jodrey–Tory generated R-packing type.

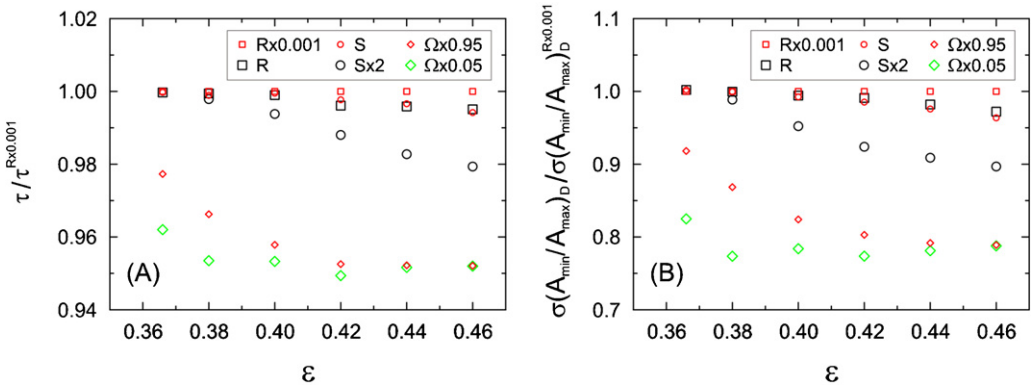

Fig. 9. Comparison between the porosity-scaling of (A) the tortuosity τ and (B) the Delaunay tessellation-based measure $\sigma(A_{min}/A_{max})_D$ for the generated packing types. Data are shown normalized to the Rx0.001-packing type.

the intensity of the spikes (and therefore the number of crystal-type pore-environments), while the functional form remains nearly unchanged.

The $(A_{min}/A_{max})_D$-distributions for the MC-packing types (Fig. 8B) are also positively skewed, but contain no spikes. Compared with JT-packings (as exemplified in Fig. 8B by the R-packing type) the $(A_{min}/A_{max})_D$-distributions of the MC-packings are visibly shifted to larger values, which range over $(A_{min}/A_{max})_D = 0.14–1$. The change in the $(A_{min}/A_{max})_D$-distributions upon densification is more pronounced for MC- than for JT-packings and accompanied by a change in the functional form, with a principal mode at lower values (for the Ωx0.95-packing at $(A_{min}/A_{max})_D = 0.38$, coinciding with the spike developed by the R-packing) and a second mode developing towards larger $(A_{min}/A_{max})_D$-values. This behavior is more pronounced for the Ωx0.05- than for the Ωx0.95-packing and again reflects the above-discussed property of the MC-algorithm to realize lower porosities by introducing dense, highly ordered regions into the packings, which leaves more possibilities (and thus more disorder) for sphere placement in the more loosely packed regions. The comparison of Fig. 8A and B reveals that MC-packings generally possess more homogeneous pore environments than JT-packings. The lower range of $(A_{min}/A_{max})_D$-values in the distributions for the JT-packings is much less realized in the MC-packings, so that their $\sigma(A_{min}/A_{max})_D$-values (Fig. 7A) and tortuosities are lower (Fig. 6).

For all six packing types $\sigma(A_{min}/A_{max})_D$ (Fig. 7A) and the tortuosity (Fig. 6) increase upon densification, which means that the extent to which the pore environment varies in a packing grows with densification and that this in turn raises the tortuosity. Fig. 9A and B shows the porosity-scaling of the simulated tortuosity values and of $\sigma(A_{min}/A_{max})_D$ side-by-side; to facilitate comparison the data are shown normalized to the Rx0.001-packing type. This direct comparison demonstrates the quality of the identified measure $\sigma(A_{min}/A_{max})_D$ as a descriptor for the porosity- and packing type-dependent influence of the packing microstructure on the diffusive tortuosity of monodisperse, bulk, random sphere packings.

4. Conclusions

By simulating diffusion in six computer-generated packing types with systematically varied degrees of microstructural heterogeneity, we have shown that the diffusive tortuosity of bulk, monodisperse, random sphere packings is not fully defined by the bed porosity, but also depends on the packing type. The tortuosity is influenced by the extent to which the structural environment of individual pores varies in a packing, and for this influence we have proposed a suitable measure based on Delaunay tessellation of the pore space. The ratio of the minimum to the maximum void face area of the Delaunay tetrahedron around a pore, $(A_{min}/A_{max})_D$, is a geometrical descriptor of the structural environment around this pore. The standard deviation of the distribution of this geometrical parameter for all pores in the packing, $\sigma(A_{min}/A_{max})_D$, follows the same porosity-scaling as the tortuosity of the investigated packing types. While $\sigma(A_{min}/A_{max})_D$ is not sufficient to predict the diffusive tortuosity of a packing, it captures the influence of the packing type with its distinct, porosity-dependent microstructure on this transport property. The identified structure–transport correlation underlines the generic difference between random and crystal hard-sphere packings: the

three-dimensionally ordered microstructure of crystal packings is independent of the porosity and has a strictly limited number of pore environments, whereas random sphere packings possess a large number of different pore environments and a correspondingly wide distribution of $(A_{min}/A_{max})_D$-values that is subject to change with porosity and packing type.

The correlation of tortuosity to the limiting properties of individual pores (*i.e.*, the ratio of minimum to maximum void face area, where the void face area may be interpreted as the size of the pore throat) reflects the piecewise, random nature of diffusion, which is calculated from independent tracer motions and knows no directional preference. This is the major difference to hydrodynamic dispersion, which depends on the convective, direction-dependent flow-field and is correlated to a packing's microstructural degree of heterogeneity (DOH) or packing-scale disorder. Packings with identical DOH (*e.g.*, R- and S-packings at $\varepsilon = 0.366$) have identical dispersion coefficients [10] as well as tortuosities, but packings with different DOHs and thus dispersion coefficients may nevertheless have identical tortuosities (*e.g.*, R- and S-packings at $\varepsilon = 0.46$). Also, a high DOH or packing-scale disorder does not necessarily indicate high tortuosity, as we have seen for the Ωx0.05-packing type at low porosities. This apparent dichotomy highlights the importance of discovering the relevant length scale of structural inhomogeneities for each transport phenomenon to establish structure–transport correlations for random porous media: packing-scale disorder for flow-field dependent dispersion *vs.* pore-environment heterogeneity for diffusion.

Acknowledgements

This work was supported by the Deutsche Forschungsgemeinschaft DFG (Bonn, Germany) under grants TA 268/4-1 and TA 268/5-1. Computational resources on IBM BlueGene®/P platforms were provided by "Genius" at RZG (Rechenzentrum Garching, Germany) and "Jugene" at FZJ (Forschungszentrum Jülich, Germany). We thank the DEISA Consortium (http://www.deisa.eu/), co-funded through the EU FP6 project RI-031513 and the FP7 project RI-222919, for support within the DEISA Extreme Computing Initiative. We are also grateful to the Jülich Supercomputing Centre (JSC) for allocation of a special CPU-time grant (project HMR10).

References

[1] J. Bear, Dynamics of Fluids in Porous Media, Elsevier, New York, 1972.
[2] F.A.L. Dullien, Porous Media – Fluid Transport and Pore Structure, Academic Press, New York, 1992.
[3] G. Guiochon, A. Felinger, A.M. Katti, D.G. Shirazi, Fundamentals of Preparative and Nonlinear Chromatography, 2nd ed., Elsevier, Amsterdam, 2006.
[4] J.S. Baker, J.C. Vinci, A.D. Moore, L.A. Colón, J. Sep. Sci. 33 (2010) 2547.
[5] F. Gritti, I. Leonardis, D. Shock, P. Stevenson, A. Shalliker, G. Guiochon, J. Chromatogr. A 1217 (2010) 1589.
[6] F. Gritti, I. Leonardis, J. Abia, G. Guiochon, J. Chromatogr. A 1217 (2010) 3819.
[7] G. Guiochon, F. Gritti, J. Chromatogr. A 1218 (2011) 1915.
[8] M.R. Schure, R.S. Maier, J. Chromatogr. A 1126 (2006) 58.
[9] S. Khirevich, A. Höltzel, A. Seidel-Morgenstern, U. Tallarek, Anal. Chem. 81 (2009) 7057.
[10] S. Khirevich, A. Daneyko, A. Höltzel, A. Seidel-Morgenstern, U. Tallarek, J. Chromatogr. A 1217 (2010) 4713.
[11] S. Bruns, T. Müllner, M. Kollmann, J. Schachtner, A. Höltzel, U. Tallarek, Anal. Chem. 82 (2010) 6569.
[12] S. Bruns, U. Tallarek, J. Chromatogr. A 1218 (2011) 1849.
[13] J.C. Giddings, Dynamics of Chromatography, Part 1: Principles and Theory, Marcel Dekker, New York, 1965.
[14] M. Barrande, R. Bouchet, R. Denoyel, Anal. Chem. 79 (2007) 9115.
[15] F.J. Valdés-Parada, M.L. Porter, B.D. Wood, Transp. Porous Media 86 (2011) 155.
[16] J.C. Maxwell, A Treatise in Electricity and Magnetism, vol. I, 2nd ed., Clarendon Press, London, 1881.
[17] B.P. Boudreau, Geochim. Cosmochim. Acta 60 (1996) 3139.
[18] L. Shen, Z. Shen, Chem. Eng. Sci. 64 (2007) 3748.
[19] M. Matyka, A. Khalili, Z. Koza, Phys. Rev. E 78 (2008) 026306.
[20] H.L. Weissberg, J. Appl. Phys. 34 (1963) 2636.
[21] E. Mauret, M. Renaud, Chem. Eng. Sci. 52 (1997) 1807.
[22] J.P. du Plessis, J.H. Masliyah, Transp. Porous Media 3 (1988) 145.
[23] M.J. Yun, B.-M. Yu, B. Zhang, M.-T. Huang, Chin. Phys. Lett. 22 (2005) 1464.
[24] P.-Y. Lanfrey, Z.V. Kuzeljevic, M.P. Dudukovic, Chem. Eng. Sci. 65 (2010) 1891.
[25] E. du Plessis, S. Woudberg, J.P. du Plessis, Chem. Eng. Sci. 65 (2010) 2541.
[26] J. Quintanilla, Polym. Eng. Sci. 39 (1999) 559.
[27] S. Torquato, Random Heterogeneous Materials – Microstructure and Macroscopic Properties, Springer Science & Business Media, LLC, New York, 2002 (Chapter 22.1).
[28] M.M. Ahmadi, S. Mohammadi, A.N. Hayati, Phys. Rev. E 83 (2011) 026312.
[29] P. Venema, R.P.W.J. Struis, J.C. Leyte, D. Bedeaux, J. Colloid Interface Sci. 141 (1991) 360.
[30] A.S. Kim, H. Chen, J. Membr. Sci. 279 (2006) 129.
[31] S. Khirevich, A. Höltzel, D. Hlushkou, U. Tallarek, Anal. Chem. 79 (2007) 9340.
[32] A. Bezrukov, M. Bargieł, D. Stoyan, Part. Part. Syst. Char. 19 (2002) 111.
[33] A.Z. Zinchenko, J. Comput. Phys. 114 (1994) 298.
[34] G.E. Schröder-Turk, W. Mickel, M. Schröter, G.W. Delaney, M. Saadatfar, T.J. Senden, K. Mecke, T. Aste, Europhys. Lett. 90 (2010) 34001.
[35] M.P. Allen, D.J. Tildesley, Computer Simulation of Liquids, Oxford University Press, 1989 (Chapter 4.4).
[36] R.S. Maier, M.R. Schure, J.P. Gage, J.D. Seymour, Water Resour. Res. 44 (2008) W06S03.
[37] F. Delay, P. Ackerer, C. Danquigny, Vadose Zone J. 4 (2005) 360.
[38] P. Szymczak, A.J.C. Ladd, Phys. Rev. E 68 (2003) 036704.
[39] H. Brenner, Phil. Trans. Roy. Soc. Lond. A 297 (1980) 81.
[40] R.S. Maier, R.S. Bernard, J. Comput. Phys. 229 (2010) 233.
[41] W. Gropp, E. Lusk, A. Skjellum, Using MPI: Portable Parallel Programming with the Message-Passing Interface, 2nd ed., MIT Press, Cambridge, MA, 1999.
[42] A. Okabe, B. Boots, K. Sugihara, S.N. Chiu, Spatial Tessellations: Concepts and Applications of Voronoi Diagrams, John Wiley & Sons Ltd., Chichester, England, 2000.
[43] C.B. Barber, D.P. Dobkin, H. Huhdanpaa, ACM Trans. Math. Softw. 22 (1996) 469.
[44] A.V. Anikeenko, N.N. Medvedev, T. Aste, Phys. Rev. E 77 (2008) 031101.
[45] S. Bryant, G. Mason, D. Mellor, J. Colloid Interface Sci. 177 (1996) 88.
[46] K.E. Thompson, H.S. Fogler, AIChE J. 43 (1997) 1377.
[47] R. Al-Raoush, K. Thompson, C.S. Willson, Soil Sci. Soc. Am. J. 67 (2003) 1687.
[48] R.Y. Yang, R.P. Zou, A.B. Yu, S.K. Choi, J. Colloid Interface Sci. 299 (2006) 719.
[49] J.Q. Xu, R.P. Zou, A.B. Yu, Granular Matter 9 (2007) 455.
[50] N. Reboul, E. Vincens, B. Cambou, Granular Matter 10 (2008) 457.
[51] S. Rémond, J.L. Gallias, A. Mizrahi, Granular Matter 10 (2008) 329.
[52] G.S. Armatas, Chem. Eng. Sci. 61 (2006) 4662.